MA_xTe_2 Phases (M = Nb, Ta; A = Si, Ge; $^1/_3 \leq x \leq {}^1/_2$): An Electronic Band Structure Calculation Analysis

Florent Boucher, Vladlen Zhukov,[†] and Michel Evain*

Laboratoire de Chimie des Solides, IMN, UMR CNRS No. 110, Université de Nantes, 2 rue de la Houssinière, 44072 Nantes Cedex 03, France

Received May 16, 1996[⊗]

The MA_xTe_2 phase (M = Nb, Ta; A = Si, Ge; $^1/_3 \leq x \leq {}^1/_2$) band structures are reexamined by means of *ab initio* LMTO-TB band structure calculations for two representative compounds, $NbGe_{1/2}Te_2$ and $NbGe_{1/3}Te_2$. Despite the high covalency of the phases, the band structures can be analyzed in terms of M d-like blocks and Te and Ge s- and p-like states. Formal oxidation states can therefore be assigned and a general formulation established. The existence of the phases is shown to emanate from a strong bonding between the A elements and their four metal neighbors. The bonding not only assures the stability of the A element in its tellurium square-like environment but also provides the stability of the lone metals in their trigonal prismatic sites, which in turn allows the commensurate or incommensurate in-plane insertion of otherwise unstable trigonal prismatic MTe_2 ribbons.

Introduction

The MA_xTe_2 phases (M = Nb, Ta and A = Si, Ge; $^1/_3 \leq x \leq {}^1/_2$) have been the object of numerous studies.[1−18] The crystal structures of both the commensurate and the incommensurate phases have been well characterized by single-crystal X-ray diffraction analyses[1−13] and later confirmed by STM and AFM surface imaging.[14−17] Two striking features of those phases are (i) the unusual presence of the A element in a square planar coordination of tellurium atoms and (ii) the one dimensional segregation of trigonal prismatic MTe_2 ribbons in MA_xTe_2 planes. Both particularities raise the question of the existence of the phases. The electronic band structures of some commensurate phases have already been calculated[4−6] by means of the extented Hückel method. The analyses established the general band pattern and revealed their nature. However, they always focused on a possible bonding character for some short Te···Te interactions across the van der Waals gap and never thoroughly discussed the other particularities of the structures. The tellurium square planar coordination of the A main group elements was said to be stabilized by the additional surrounding of A by four metals at short distances, but no precise studies were done on how this stabilization was achieved. On the other hand, the peculiarity of the niobium or tantalum MTe_2 trigonal prismatic ribbons was not tackled, although it is a key feature of the MA_xTe_2 phases ($^1/_3 \leq x < {}^1/_2$). The (quasi) periodicity of such a ribbon controls the commensurability of the phase and the absence of two such ribbons side by side gives the lower limit of the A content ($x = {}^1/_3$). However, niobium and tantalum metals are not stable in trigonal prismatic coordinations in the presence of tellurium and prefer octahedral sites, as in the MTe_2 binary phases for instance. To understand the formation of the MA_xTe_2 phases the electronic band structures of several end members ($x = {}^1/_3$ or $^1/_2$; A = Si, Ge; M = Nb, Ta) have been recalculated and analyzed by means of the self-consistent *ab initio* linear muffin-tin orbital method in the tight-binding representation (LMTO-TB). The results obtained for the most covalent representatives, $NbGe_{1/2}Te_2$ and $NbGe_{1/3}Te_2$, are presented in this report.

I. Computational Aspects

The LMTO-TB method is described in detail in refs 19−22. The method splits the crystal space into overlapping atomic spheres (Wigner−Seitz spheres), whose radii are chosen to completely fill the crystal volume. In the present calculations, additional empty spheres (E) had to be included to model the van der Waals gap. The search

[†] On leave from the Institute of Solid State Chemistry, Urals Branch of the Academy of Sciences, Pervomayskaya 91, 620219 Ekaterinburg, Russia.

[⊗] Abstract published in *Advance ACS Abstracts,* November 15, 1996.

(1) Monconduit, L.; Evain, M.; Boucher, F.; Brec, R.; J. Rouxel *Z. Anorg. Allg. Chem.* **1992**, *616*, 177.
(2) Li, J.; Caroll, P. J. *Mater. Res. Bull.* **1992**, *27*, 1073.
(3) Li, J.; Badding, M. E.; Disalvo, F. J. *J. Alloys Compd.* **1992**, *184*, 257.
(4) Monconduit, L.; Evain, M.; Brec, R.; Rouxel, J.; Canadell, E. *C. R. Acad. Sci. Paris Ser. 2* **1993**, *316*, 25.
(5) Canadell, E.; Monconduit, L.; Evain, M.; Brec, R.; Rouxel, J.; Whangbo, M.-H. *Inorg. Chem.* **1993**, *32*, 10.
(6) Evain, M.; Monconduit, L.; Van der Lee, A.; Brec, R.; Rouxel, J.; Canadell, E. *New J. Chem.* **1994**, *18*, 215.
(7) Van der Lee, A.; Evain, M.; Mansuetto, M.; Monconduit, L.; Brec, R.; Rouxel, J. *J. Solid State Chem.* **1994**, *111*, 75.
(8) Van der Lee, A.; Evain, M.; Monconduit, L.; Brec, R.; van Smaalen, S. *J. Phys. Condens. Matter* **1994**, *6*, 933.
(9) Van der Lee, A.; Evain, M.; Monconduit, L.; Brec, R.; Rouxel, J.; Petříček, V. *Acta Crystallogr., Sect. B* **1994**, *50*, 119.
(10) Evain, M.; Van der Lee, A.; Monconduit, L.; Petříček, V. *Chem. Mater.* **1994**, *6*, 1776.
(11) Van der Lee, A.; Evain, M. In *Aperiodic '94;* Chapuis, G., Paciorek, W., Eds.; World Scientific Publishing: River Edge, NJ, 1995; p 440.
(12) Boucher, F.; Evain, M.; Petříček, V. *Acta Crystallogr., Sect. B* **1996**, *52*, 100.
(13) Gareh, J.; Boucher, F.; Evain, M. *Eur. J. Solid State Inorg. Chem.* **1996**, *33*, 355.
(14) Liang, W.; Whangbo, M. -H.; Evain, M.; Monconduit, L.; Brec, R.; Bengel, H.; Cantow, H. -J.; Magonov, S. N. *Chem. Mater.* **1994**, *6*, 678.
(15) Bengel, H.; Cantow, H. -J.; Magonov, S. N.; Monconduit, L.; Evain, M.; Liang, W.; Whangbo, M. -H. *Adv. Mater.* **1994**, *6*, 649.
(16) Bengel, H.; Cantow, H. -J.; Magonov, S. N.; Monconduit, L.; Evain, M.; Whangbo, M. -H. *Surf. Sci.* **1994**, *321*, L170.
(17) Bengel, H.; Cantow, H. -J.; Evain, M.; Magonov, S. N.; Whangbo, M. -H. *Adv. Mater.* in press.
(18) Tremel, W.; Kleinke, H.; Derstroff, V.; Reisner, C. *J. Alloys Compd.* **1995**, *219*, 73.
(19) Andersen, O. K. In *The Electronic Structure of Complex Systems*; Phariseau, P., Temmerman, W. M., Eds.; Plenum Publishing Corporation: New York, 1984; p 11.
(20) Lambrecht, W. R. L.; Andersen, O. K. *Phys. Rev. B* **1986**, *34*, 2439.
(21) Andersen, O. K.; Jepsen, O.; Sob, M. In *Electronic Band Structure and Its Applications*; Yussouf, M., Ed.; Springer-Verlag: Berlin, 1986; p 1.
(22) Andersen, O. K.; Pawlowska, Z.; Jepsen, O. *Phys. Rev. B* **1986**, *34*, 5253.

S0020-1669(96)00564-2 CCC: $12.00

Table 1. Positions and Radii (Å) of the Wigner−Seitz and Empty Spheres

	$NbGe_{1/2}Te_2$				$NbGe_{1/3}Te_2$				
	x	*y*	*z*	*R* (Å)		*x*	*y*	*z*	*R* (Å)
Nb1	0.2500	0.2863	0.1075	1.623	Nb1	0.3265	1/4	0.6669	1.631
Nb2	0.2505	−0.0350	−0.1054	1.633	Nb2	0.0340	1/4	0.3136	1.616
Ge	0.2510	0.1250	0.4990	1.538	Nb3	0.3048	1/4	0.9674	1.573
Te1	0.3845	0.0121	0.2590	1.671	Ge	0.4250	1/4	0.4250	1.524
Te2	0.1158	0.2378	−0.2548	1.675	Te1	0.2104	0.1154	0.1582	1.652
Te3	0.3846	0.5120	0.3254	1.667	Te2	0.1397	0.1189	0.5050	1.662
Te4	0.1164	−0.2598	−0.3274	1.658	Te3	0.1463	0.1141	0.8188	1.615
E1	0	0	1/2	1.575	E1	0	0	0	1.575
E2	−0.0174	0.2553	0.0033	1.456	E2	0.4557	−0.0065	−0.1753	1.405
E3	0	1/2	1/2	1.238	E3	−0.1466	0.0729	0.1596	1.096
E4	0.0575	1/4	0.3702	1.150	E4	0.1820	−0.0513	0.1615	1.048
E5	−0.0548	0.4974	0.1458	1.131	E5	0.3190	0.0524	−0.0299	0.980
E6	−0.0495	0.2218	−0.3281	1.035	E6	0.4973	0.1896	−0.1708	0.963
E7	0.0542	−0.0385	−0.1662	0.993	E7	−0.0401	0.1423	−0.0380	0.795
E8	−0.1428	−0.0398	−0.4984	0.814					
E9	0.1489	−0.2455	0.1276	0.808					

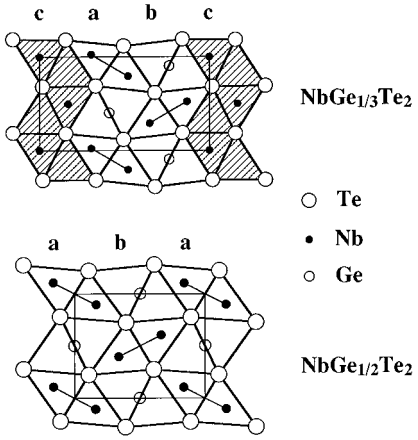

Figure 1. Projections of one slab of the $NbGe_{1/3}Te_2$ (a) and $NbGe_{1/2}Te_2$ (b) structures. For convenience, in both figures the origin has been chosen in accordance with the calculations and is nonconventional.

for both the optimum positions of the empty spheres and the optimum radii of the atomic spheres was performed using the automatic procedure reported in ref 23. The positions and radii of the Wigner−Seitz and those E spheres are given in Table 1. The short-range muffin-tin orbitals included in the calculations were the 5s, 5p, 4d, and 4f states of Nb, the 5s, 5p, 5d, and 4f states of Te, the 4s, 4p, and 4d states of Ge, and the s, p, and d states of E. The Nb f, Te d−f, Ge d, and E p−d states were "down-folded" using Lowdin's technique.[20] The calculations included combined-correction terms[21] and were performed with 266 and 325 irreducible *k*-points for $NbGe_{1/2}Te_2$ and $NbGe_{1/3}Te_2$, respectively.

II. Crystal Structures

The MA_xTe_2 structures have been described in detail in several papers.[1−4,6−13] They are based upon the stacking of tellurium trigonal prismatic slabs. There are two such slabs per unit cell with the stacking varying from one phase to another, e.g. orthorhombic (AA)(BB) for $NbGe_{1/3}Te_2$ and monoclinic (AA)(BB)(CC) for $NbGe_{1/2}Te_2$. The metals M and main elements A occupy different sites within the trigonal prismatic layers. The van der Waals gaps (with octahedral voids) separating the slabs give the compounds a classical layered character. The originality of the phases lies in the facts that, within the slabs, some M atoms form M_2 pairs, other M atoms are isolated, and the A elements adopt an unusual square planar coordination (see Figure 1). This arrangement divides the layers in three different ribbon types, called **a**, **b**, and **c**. The **a** and **b** ribbons, with the formulation $MA_{1/2}Te_2$, are equivalent and host the M_2 metal pairs and the A main elements, while the **c** ribbons, with the formulation MTe_2, accommodate the lone metals. It is the periodicity of the **c** ribbons that determines the stoichiometry and the commensurate or incommensurate character of the phases. An ···−abc−abc−··· ribbon succession is found in $NbGe_{1/3}Te_2$.

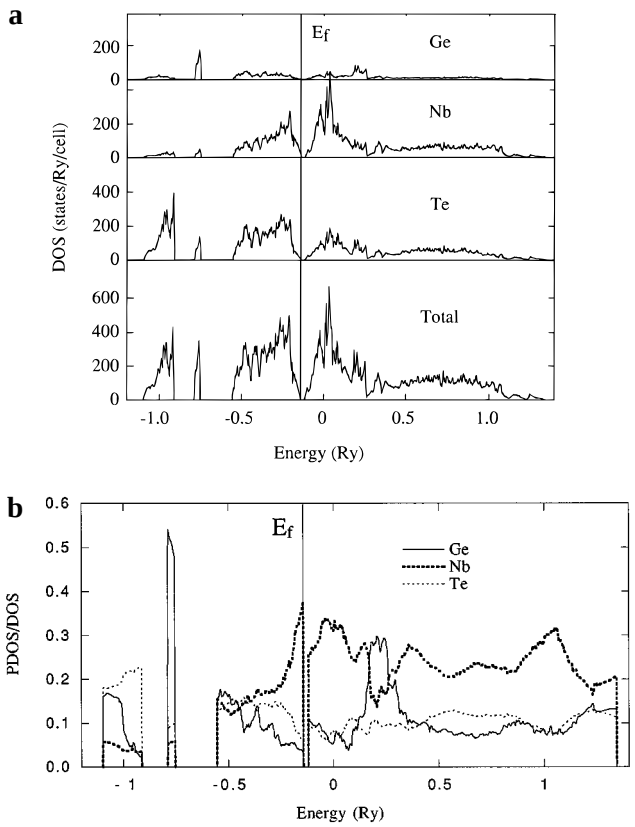

Figure 2. (a) Total density of states and Ge, Te, and Nb projected density of states of $NbGe_{1/2}Te_2$. (b) Relative projected density of states (see text) per Nb, Ge, and Te atom of $NbGe_{1/2}Te_2$.

III. Band Structure Results

$NbGe_{1/2}Te_2$. The total density of states (DOS) and partial density of states (PDOS) of $NbGe_{1/2}Te_2$ are depicted in Figure 2a. The assignment of the low-lying energy bands is straightforward (the decomposition in s, p, and d states, although performed, is not shown for brevity). The first band between −1.1 and −0.9 Ry consists primarily of Te 5s states and the next narrow band near −0.75 Ry is composed mainly of Ge 4s

(23) Jepsen, O.; Andersen, O. K. *Z. Phys. B* **1995**, *97*, 35.

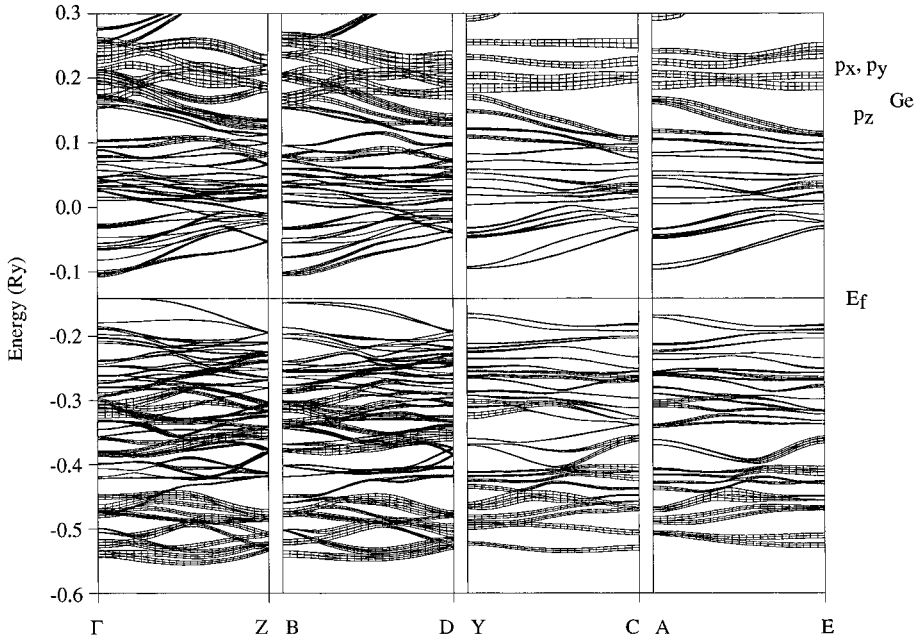

Figure 3. Fat bands for the Ge 4p states of $NbGe_{1/2}Te_2$ in the energy region between −0.6 and +0.3 Ry, where Γ = (0,0,0), A = ($^1/_2$,−$^1/_2$,0), B = ($^1/_2$,0,0), C = (0,$^1/_2$,$^1/_2$), D = ($^1/_2$,0,$^1/_2$), E = ($^1/_2$,−$^1/_2$,$^1/_2$), Y = (0,$^1/_2$,0), and Z = (0,0,$^1/_2$).

states. However, the continuum of states in the interval between −0.55 Ry and the Fermi level at −0.14 Ry is more complicated in nature. A better comprehension of the atomic characters of that band is obtained by looking at the relative projected densities of states (RPDOS) per atom presented in Figure 2b. The RPDOS curves, which give the integrated (over the Brillouin zone) orbital characters of a given atom (or atomic class) as a function of energy, are less cumbersome than the usual more instructive "fat band" curves, which give the orbital character weighted band structure. It is clear that the Te 5p components are more important in the lower part of the band, in the −0.55 to −0.25 Ry energy range, than at the top of the band where the Nb 4d state characters dominate. The mixing of Ge 4p states is also important, in particular at the low-energy region of the band. Notice that, once again, the s, p, or d orbital characters for each element have been determined with distinct s, p, or d RPDOS (not shown for brevity).

The next energy band is separated from the Fermi level by the forbidden gap, 0.023 Ry wide. The band can be decomposed in three sub-bands. The low energy sub-band is primarily built upon Nb-like states; it spreads out up to 0.15 Ry in energy (see Figure 2a). As revealed by Figure 2b, the next sub-band around 0.2 Ry is chiefly composed of the Ge 4p states. Finally the Nb 5s states emerge in the remainder of the band above 0.25 Ry.

A basis for the rationalization of the Nb-like states is provided in ref 4 where the results of extended Hückel tight binding (EHTB) calculations for the parent compound Nb_2SiTe_4 are discussed. According to the authors' arguments, the lowest d-block level of the Nb_2 unit is related to the σ_+-bonding between the in-plane d_{z^2} orbitals—with the *z* axis along the bond—and the next d-block level can be referred to the δ_- antibonding between the $d_{x^2-y^2}$ states as depicted in **1** (notice

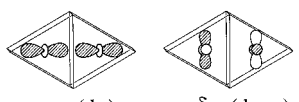

1

that different axis orientations will be used for different structural fragments throughout the text). EHTB calculations performed on a small cluster are certainly insufficiently precise to correctly foresee the energies of such states in the extended structure. Indeed, analyses of the LMTO-TB crystal orbital characters by means of the fat bands and of plots of the crystal orbitals at several special Brillouin zone *k* points reveal that the situation is far more complex. From those analyses it can be inferred that the lowest d-block levels of the Nb_2 unit chiefly correspond to the combinations presented in **2**. The slight difference comes

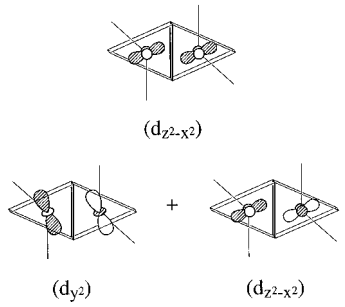

2

from the fact that the short central Te−Te contacts (*ca.* 3.3 Å) and the four germanium capping atoms are not taken into account in ref 4. In fact the actual situation resembles that presented in ref 24 for a bicapped trigonal bipyramidal M_2S_{12} coordination with two central S_2 pairs. However, the situation is more complicated in the present structure because the Nb_2 d-block bands are antibonding with respect to tellurium but bonding with respect to germanium (this was easily verified with ρ map analyses). One can nevertheless conclude that the eight highest occupied crystal orbitals of the band structure (see Figure 3) are Nb d-like states. Therefore, since there are eight Nb metals per unit cell, the formal charge balance for $NbGe_{1/2}Te_2$ can be written as $Nb^{III}{}_2Ge^{II}Te^{-II}{}_4$. This is of course purely formal and far from the real charge equilibrium because of the strong orbital mixing.

The fat bands for Ge 4p states are shown in Figure 3. Their width is well pronounced throughout the whole Te 5p-like band,

(24) Evain, M.; Brec, R.; Whangbo, M. -H. *J. Solid State Chem.* **1987**, *71*, 244.

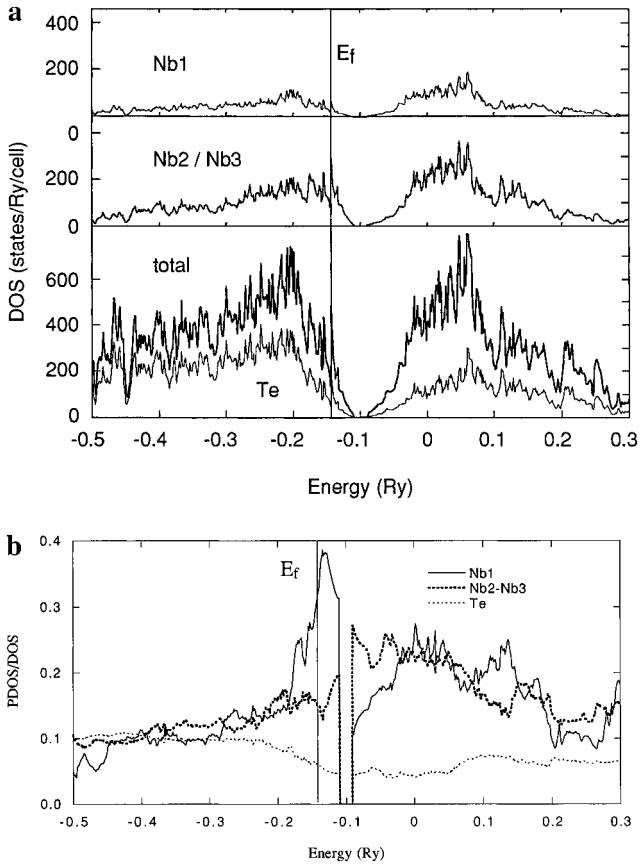

Figure 4. (a) Total density of states and Te, Nb2−Nb3, and Nb1 projected density of states of $NbGe_{1/3}Te_2$. (b) Relative projected density of states (see text) per Nb and Te atom of $NbGe_{1/3}Te_2$.

at the bottom of the valence band from −0.55 to −0.25 Ry, thus revealing a strong Te-5p/Ge-4p hybridization. This is also clear in Figure 2b where the Ge RPDOS is almost as strong as that of Nb. This is also a difference with the EHTB calculations which apparently showed no significant contribution of the A main element in the vicinity of the Fermi level. Considering that bonding hybridization is provided by the Ge p orbitals pointing toward the four tellurium atoms of the $GeTe_4$ square, one expects two antibonding states per germanium atom with strong Ge components. By rotation of the coordination axes to bring the *z* axis perpendicular to the $GeTe_4$ square, eight such states (2 × 4Ge) are indeed found in the energy interval between 0.18 and 0.28 Ry. Obviously the remaining Ge p_z orbital does not provide a good overlap with the Te atoms; therefore it gives rise to four bands at lower energy, between 0.1 and 0.18 Ry. This p_z orbital can however lead to a partial overlap with the orbitals of the four capping metals that have a proper orientation (d_{y^2} of **2** for instance). Such a hybridization is observed for the four bands. Besides, the Nb-like bands near 0.1 Ry contain a component of Ge states which can be attributed to Nb−Ge bonding. This bonding−antibonding is however purely formal, with the states being empty and hence not influencing the chemical bonding. It is worth noticing that the hybridization between the Nb 5d states and the Ge 4p states is very small at the top of the valence band, where the Nb states are predominant. The reason is an unfavorable orientation of the Nb_2 orbitals with respect to the Ge atoms (except for d_{y^2}).

$NbGe_{1/3}Te_2$. The DOS and the Te, Nb2−Nb3, and Nb1 PDOS of $NbGe_{1/3}Te_2$ are presented in Figure 4a. A distinction has been made between the metal in the Nb_2 entities (Nb2 and Nb3) and the lone metals (Nb1). Furthermore, the bands in the energy region between −1.2 and −0.7 Ry have been omitted since they are very similar to those of $NbGe_{1/2}Te_2$. The curves reveal that the Te 5p states dominates from −0.55 Ry up to −0.2 Ry whereas the Nb-like states take over at higher energy. Once again, this is more obvious in the RPDOS curves gathered in Figure 4b. The Fermi level cuts the Nb-like states at 0.14 Ry, thus implying a compound with a metal character. The next set of Nb-like bands is separated by a gap centered at *ca.* −0.1 Ry and continues up 0.2 Ry. Then come the Ge 4p states which dominate up to 0.25 Ry (not presented in figure 4).

From this description it appears that the band structure of $NbGe_{1/3}Te_2$ is very similar to that of $NbGe_{1/2}Te_2$. The essential differences are the position of the Fermi level and the nature of the Nb states near the Fermi level. A comparison of the Nb2−Nb3 and Nb1 RPDOS (see Figure 4b) shows that the weight of the Nb1 atoms is markedly larger than that of Nb2−Nb3 in the four last bands of the valence band, at energies just below (two bands) and just above (two bands) the Fermi level. This is also what can be observed in the Nb fat band structures (not shown). Therefore, it is possible to assert that the two depleted crystal states belong preferably to the lone Nb1 metals. Further down, in the interval between −0.19 and −0.14 Ry, eight bands have a strong Nb2−Nb3 character. So the formal d-state configurations of the niobium atoms are $4d^1$ for Nb1 and $4d^2$ for Nb2 and Nb3, and thus the charge equilibrium is $(Nb^{III}_2)Nb^{IV}Ge^{II}Te^{-II}_6$. Once again, such a charge balance is established by completely neglecting the hybridizations, which are very important in the MA_xTe_2 phases. In previous reports,[4−6] the same +III oxidation state was given to the different metals.

In ref 6, it was stated that the d_{z^2} level (**3**) was the lowest d-block level for the lone Nb1 metals. Once again, the actual situation is significantly different because of the germanium atom, which caps the trigonal prism in a very special way. As a result, the lowest Nb1 state takes a more $d_{z^2-y^2}$-like (**4**)

3 **4**

character. This is observed both in EHTB calculations and in the analysis of the LMTO-TB results by means of the fat bands and of the plot of the crystal orbitals at various special Brillouin zone *k* points.

IV. Charge Densities and Chemical Bonding

The significance of the short Te···Te interslab contacts in the MA_xTe_2 phases has already been discussed in detail.[25] However, the stability of the A element in its tellurium square coordination and of the lone Nb or Ta metals in their tellurium prismatic environments have not yet been thoroughly analyzed. Since they seem to be key issues in the formation of all the MA_xTe_2 phases (M = Nb, Ta and A = Si, Ge; $^1/_3 \leq x \leq {}^1/_2$), they will both be discussed.

In Figure 5a is shown an electron density map for $NbGe_{1/2}Te_2$ showing the tellurium square-like coordination of germanium. Strong deviations from spherical atomic symmetry is obvious, with a concentration of charge density (*ca.* 0.046 e^-/au^3) along the Ge-Te directions ($d_{Ge-Te} \sim 2.78$ Å). This confirms the existence of bonding between germanium and tellurium within the square. Although the energy interval between Ge 4p and Te 5p atomic states is large, the hybridization is favored because

(25) Evain, M.; Monconduit, L.; Brec, R. *J. Solid State. Chem.* **1995**, *119*, 394.

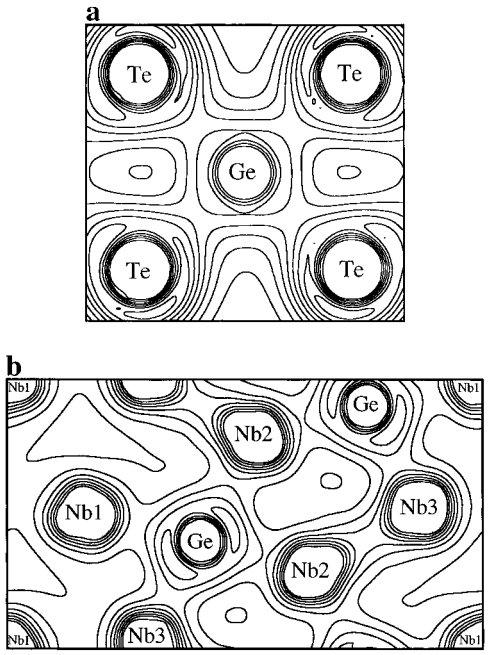

Figure 5. Contour maps of the electron density ρ for (a) a section from the $NbGe_{1/2}Te_2$ structure showing the tellurium square-like coordination of germanium and (b) a section from the $NbGe_{1/3}Te_2$ structure, parallel to the slab and containing both the metals and the germanium atoms. Contour lines are from 0.01 (a) and 0.02 (b) e^-/au^3 in intervals of 0.01 e^-/au^3 (core levels have been hidden for clarity).

of the rather diffuse nature of the Te 5p orbitals. While the Ge-Te antibonding Ge 4p-like states around 0.23 Ry are empty, the Te 5p-like counterparts are filled and provide the bonding electrons.

A similar map is presented in Figure 5b for $NbGe_{1/3}Te_2$, but for a section parallel to the slab and containing both the metals and the *A* main elements. For the Nb_2 dimers ($d_{Nb-Nb} \sim 2.92$ Å), a bonding area is observed between the niobium atoms, with an electron density of *ca.* 0.054 e^-/au^3. This is obviously related to the σ_+ bonding presented in **2**. For the germanium surroundings, intersite regions of high electron density (average saddle point value of *ca.* 0.040 e^-/au^3) are found in two distinct regions between the germanium atoms and the four niobium atoms ($d_{Ge-Nb} \sim 2.81$ Å). They are located near the center of the two empty prisms on both sides of the $GeTe_4$ group. Since the germanium s or p character is small in the niobium d-block band, the question of the origin of the bonding is raised. To answer that question, electron density calculations have been performed in two different energy windows, one at the bottom of the valence band corresponding to the Te 5p-like block and another one at the top of the valence band up to the Fermi level corresponding to the Nb 4d-like states. The two electron density maps are presented in parts a and b of Figure 6, respectively. It is clear that the germanium to niobium bonding occurs in the bottom part of the valence band, which means that it has a through-bond nature. Indeed, no significant Ge−Nb bonding is observed in Figure 6b, in agreement with the fact that the Ge states have a low direct mixing order with the Nb d states, most of the bonding arising in the tellurium p-band where both Ge and Nb contribute. Finally, a weak bonding is observed between the Nb1 lone metal and the Nb2−Nb3 pairs. This bonding is revealed by the deformation of the electron density maps in Figure 6b.

Figure 7 presents the electron density of the tellurium plane constituting the trigonal prismatic slabs. Within that plane the Te−Te distances range from 3.3 Å (solid line) to 4.1 Å (broken line). The shortest distance was calculated as bonding in the

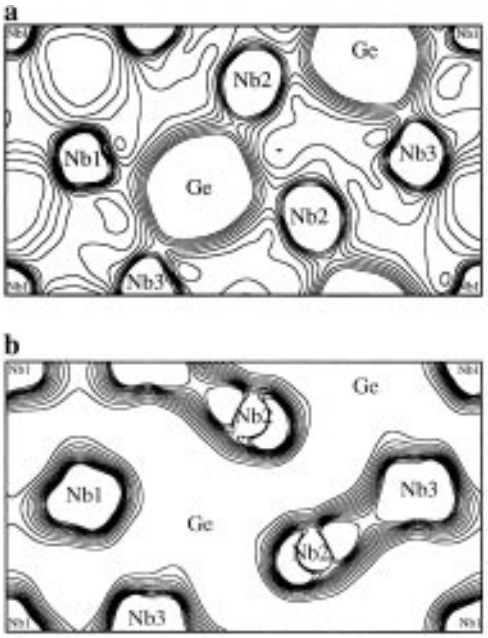

Figure 6. Contour maps of the electron density ρ of the Nb/Ge plane (a) integrated over the Te p-like block (−0.55, −0.25 Ry) and (b) integrated over the Nb d-like block (−0.25, −0.14 Ry). Contour lines are from 0.01 e^-/au^3 in intervals of 0.0025 e^-/au^3 (core levels have been hidden for clarity).

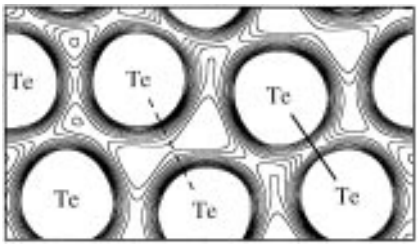

Figure 7. Contour map of the electron density ρ of the Te planes. The longest and shortest Te···Te contacts are indicated by a broken and solid line, respectively. Contour lines are from 0.01 e^-/au^3 in intervals of 0.0025 e^-/au^3 (core levels have been hidden for clarity).

EHTB calculations.[5,6] This is confirmed by our LMTO-TB calculations since the electron density, although weak, is reinforced in between the tellurium atoms of the short Te···Te contacts. Deformations of the electron density are also observed for the longest distances. This was not suggested by the EHTB calculations. The reason for those weak bonding interactions results from the presence of a strong component of the antibonding states of the Te···Te contacts within the Nb empty d levels.

The formation of the MA_xTe_2 phase can thus easily be understood. The *A* element in its tellurium square environment is stabilized not only by an effective A−Te covalent bonding, but also by through-bond interactions with the four surrounding M metals. The indirect A−M bonding interactions are also essential for the stability of the lone M metals in a prismatic tellurium coordination for the phases with $x < 1/2$. For all the MA_xTe_2 structures with **c** ribbons, i.e. with $x < 1/2$, each lone M metal of the **c** ribbons is linked to one A atom (see Figure 1).

Concluding Remarks

The *ab initio* LMTO-TB electronic band structure calculations that were performed highlight new elements that help understand the formation of the MA_xTe_2 phases. Although highly covalent in nature, the band structure can be analyzed in terms of blocks.

The M and A s-like blocks stands well below the Fermi level. The M d-like block is embedded between the Te and Ge p-like states, at the Fermi level. Furthermore, the lone metal levels can be differentiated from those of the M_2 dimers, especially around the Fermi energy. It is therefore possible to assign formal oxidation states and to establish a crude charge balance for all x values, rational or irrational. This charge balance can be written as $[(M^{III}{}_2)_xA^{II}{}_xTe^{-II}{}_{4x}][M^{IV}{}_{1-2x}Te^{-II}{}_{2-4x}]$ to stress the neutrality of the MTe_2 **c** ribbons. The key feature that assures the formation of the MA_xTe_2 phases is the main element (Si or Ge) to metal (Nb or Ta) bonding. It not only assures the stability of the main element in its tellurium square-like environment, but it also provides the stability of the lone metals in their trigonal prismatic sites. Without this last stabilization, the **c** ribbons would probably not be stable. This is supported by the fact that no structures with two **c** ribbons side by side have been found so far, even in the presence of in-plane disorder.[17] Finally, the short Te···Te contacts (3.3 Å) are demonstrated as being bonding contacts. The fact that all the tellurium atoms, except those in the **c** ribbons, are involved in such bonding dimers leads to an important charge transfer from the tellurium to the metal (not included in the writing of the formal charge balance), which is thought to further stabilize the phases.

Acknowledgment. The authors are grateful to Professor O. K. Andersen for providing his LMTO-TB program.

IC960564X